Available online at www.sciencedirect.com
ScienceDirect
International Journal of Heat and Mass Transfer 50 (2007) 605–615
International Journal of HEAT and MASS TRANSFER
www.elsevier.com/locate/ijhmt

Buoyant convection in an enclosure under time-periodic magnetizing force

Dong Gu Kang [a], Jae Min Hyun [b,*]

[a] Safety Issue Research Department, Regulatory Research Division, Korea Institute of Nuclear Safety, 19 Kusong-dong, Yusong-gu, Daejeon 305-338, South Korea
[b] Department of Mechanical Engineering, Korea Advanced Institute of Science and Technology, 373-1 Kusong-dong, Yusong-gu, Daejeon 305-701, South Korea

Received 14 December 2005; received in revised form 15 July 2006
Available online 13 October 2006

Abstract

A numerical study is made of buoyant convection of air in an enclosure under constant gravity and time-periodic magnetizing force. Buoyant convection occurs when the two vertical sidewalls are maintained at different temperatures and the horizontal walls are thermally insulated. To this basic layout, electric coils are located at the left and right sides of the cavity for case 1. For case 2, the electric coils are located below and above the cavity. The currents in the coils are activated in an alternating fashion. Comprehensive numerical solutions are found for the time-dependent Navier–Stokes equations, which include the magnetizing force term. The computed results reveal the existence of resonance, which is characterized by maximal amplification of the fluctuations of heat transfer in the interior. This resonance phenomenon is apparent when the basic mode of internal gravity oscillation is excited. The augmentation and/or suppression of convective activities by the action of magnetizing force is the primary factor to induce resonance. The configuration of case 1 is seen to be more effective than that of case 2 in heat transfer enhancement.

1. Introduction

The advent of superconducting materials paves the way to produce a very strong magnetic field in the laboratory. Extensive investigations are underway to probe the fluid flow and heat transfer of an engineering system under substantial magnetic influence. The behavior of an electrically conducting fluid subjected to the Lorentz force, which leads to magneto-hydrodynamics, has been widely studied. However, only recently the flow features of an electrically non-conducting fluid under magnetizing force have been under investigation. In particular, oxygen is an important paramagnetic material. Therefore, air is often used as the working fluid in the study of the effect of magnetizing force in convective heat transfer analyses.

Braithwaite et al. [1] considered facilitation or suppression of buoyancy-driven convection by use of a magnetic field. Wakayama [2,3] demonstrated the analogousness of the roles of magnetizing force and conventional gravity force, which can be utilized to enhance the overall convective heat transfer. Similarly, Tagawa et al. [4–6] presented complete mathematical formulations for flow of a non-conducting fluid, which include the magnetizing force. A brief scan of these previous efforts [1–6] asserts that the magnetizing force can indeed be utilized like the gravity force, and the global fluid system may be effectively controlled by imposing a magnetic field. The majority of preceding studies have dealt with the steady-state situations. The response of the fluid system to time-dependent magnetizing effect has not been fully examined. This issue is significant from the standpoint of heat transfer enhancement.

In ordinary gravity-driven natural convection of a non-magnetized fluid system, it has been shown that heat transfer augmentation is possible by choosing an appropriate

* Corresponding author. Tel.: +82 42 869 3012; fax: +82 42 869 3210.
E-mail address: jmhyun@kaist.ac.kr (J.M. Hyun).

0017-9310/$ - see front matter © 2006 Elsevier Ltd. All rights reserved.
doi:10.1016/j.ijheatmasstransfer.2006.07.014

Nomenclature

A	aspect ratio
$\vec{b}$, $\vec{B}$	dimensional and non-dimensional magnetic induction [T]
b_a	$\mu_m i/H$ [T]
d	diameter of the electric coil [m]
e	distance between the electric coil and the cavity [m]
f	frequency of the periodic magnetizing force [1/s]
$\vec{f}_m$	magnetizing force, Eq. (2) [N/m^3]
g	gravity [m/s^2]
H	height of the cavity [m]
i	electric current in the coil [A]
L	width of the cavity [m]
p, P	dimensional and non-dimensional pressure [Pa]
Pr	Prandtl number
$\vec{r}$, $\vec{R}$	dimensional and non-dimensional position vector [m]
Ra	Rayleigh number
$\vec{s}$, $\vec{S}$	dimensional and non-dimensional periphery line of the coil [m]
$d\vec{s}$, $d\vec{S}$	dimensional and non-dimensional tangential vector element of the coil [m]
t	time [s]
T	temperature [K]
T_0	average temperature, $(T_h + T_c)/2$ [K]
ΔT	temperature difference [K]
u, v	velocity in the x-, y-direction [m/s]
U, V	non-dimensional velocity in the X-, Y-direction
$\vec{V}$	non-dimensional velocity vector
x, y	Cartesian coordinates [m]
X, Y	non-dimensional Cartesian coordinates

Greek symbols

α	volumetric expansion coefficient [1/K]
χ	mass magnetic susceptibility [m^3/kg]
γ	relative magnetic effect
κ	thermal diffusivity of fluid [m^2/s]
μ_m	magnetic permeability in a vacuum [H/m]
ν	kinematic viscosity of fluid [m^2/s]
θ	non-dimensional temperature
ρ	density [kg/m^3]
τ	non-dimensional time
ψ	non-dimensional stream function
ω	non-dimensional frequency of the periodic magnetizing force, $\omega = f \Big/ \left((RaPr)^{1/2} \frac{\kappa}{H^2} \right)$

Subscripts

C	cold wall ($X = 0$)
H	hot wall ($X = 1$)
M	vertical mid-plane ($X = 0.5$)
r	resonance
ss	basic state

value of frequency in the externally applied time-dependent boundary conditions [7–13]. The crux of the argument is that the convective heat transfer is maximized when a characteristic frequency of the system is excited. This can be accomplished by tuning in a proper value of the forcing frequency of the time-dependent, externally controllable boundary temperature variations. This represents resonance of the system [7–9], and the task is to identify the characteristic frequencies of the system. In the case of a gravity-driven buoyant convection of a non-magnetized fluid at large Rayleigh number, the basic characteristic frequency has been shown to be the internal gravity oscillations [10–13]. The analysis was shown to be consistent with the numerical predictions [10–13].

The purpose of this study is to explore the flow and heat transfer features of a confined buoyant convective system of an electrically non-conducting fluid when the externally applied magnetic field is time-periodic. A differentially heated square cavity is adopted, which is placed in the usual gravity field. Numerical solutions to the time-dependent Navier–Stokes equations, which take into account the magnetizing force term, are acquired.

The overall convective flow and thermal patterns over a cycle are illustrated. The response of the fluid system to the change in location of the electrical coil is carefully monitored. The numerical results point to the existence of resonance and the resonance frequency is found to be compatible with the physical reasoning. It is comparatively easy to control electrically the strength of time-periodic magnetic field. This suggests practical utilizations in heat transfer enhancement by applying the time-periodic magnetic field tuned to the resonance frequency.

2. Formulation and numerical model

Consider a square cavity, i.e., the aspect ratio, $H/L = 1.0$, filled with an incompressible Boussinesq fluid. The gravity acts downward, and the top and bottom endwalls are thermally insulated. The temperatures at the left ($x = 0$) and right ($x = L$) vertical sidewalls are respectively T_C and T_H ($\equiv T_C + \Delta T$, $\Delta T > 0$). This basic flow layout represents the benchmark side-heated square cavity [14]. In the present study, the magnetic field is applied externally by placing two sets of electrical coil of diameter d, as sketched in Fig. 1.

Two cases of geometrical arrangement of coil are considered: case 1, the coils are located at the horizontal distance e from the sidewalls, i.e., $x = -e$, $x = L + e$; case 2, the coils are located at the vertical distance e from the horizontal endwalls, i.e., $y = -e$, $y = H + e$.

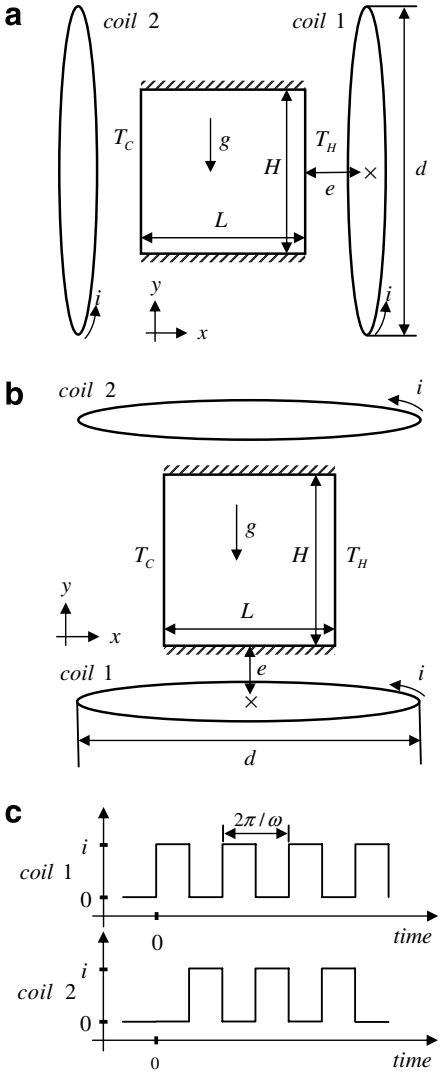

Fig. 1. (a) Flow configuration (case 1), (b) flow configuration (case 2) and (c) time-periodic electric current.

The magnetic field $\vec{b}$ induced by the electrical coil, carrying current i, is calculated by the Biot–Savart's law, i.e.,

$$\vec{b} = -\frac{\mu_m i}{4\pi}\oint \frac{\vec{r}\times d\vec{s}}{r^3}, \tag{1}$$

in which μ_m denotes the magnetic permeability of fluid, and $\vec{r}$ is the position vector of the coil element $d\vec{s}$.

The magnetizing force $\vec{f}_m$, in the magnetic field $\vec{b}$, is expressed as

$$\vec{f}_m = \frac{\rho\chi}{2\mu_m}\vec{\nabla} b^2. \tag{2}$$

In the above, ρ is the density of fluid, and χ is the mass magnetic susceptibility. As seen, for a paramagnetic substance, the mass magnetic susceptibility χ is inversely proportional to the absolute temperature, i.e., $\chi \propto 1/T$, which is known as Curie's law. Therefore, when there is temperature inequality in the system, fluid motions are generated by the magnetizing force [1–6].

The governing equations can be obtained by incorporating the magnetic force term as an additional body force in the Navier–Stokes equations [4–6]. These, in the properly non-dimensionalized form, are

$$\nabla\cdot\vec{V} = 0, \tag{3}$$

$$\frac{D\vec{V}}{D\tau} = -\nabla P + \left(\frac{Pr}{Ra}\right)^{1/2}\nabla^2\vec{V} + \theta\left[-\gamma(F_1(\tau)\nabla B_1^2 + F_2(\tau)\nabla B_2^2) + \begin{pmatrix}0\\1\end{pmatrix}\right], \tag{4}$$

$$\frac{D\theta}{D\tau} = \left(\frac{1}{PrRa}\right)^{1/2}\nabla^2\theta, \tag{5}$$

$$\vec{B} = -\frac{1}{4\pi}\oint\frac{\vec{R}\times d\vec{S}}{R^3}. \tag{6}$$

Non-dimensionalization has been implemented as

$$\tau = t(RaPr)^{1/2}\frac{\kappa}{H^2},\quad (X,Y) = \frac{(x,y)}{H},$$
$$(U,V) = (u,v)(RaPr)^{-1/2}\frac{H}{\kappa},\quad \theta = \frac{T-T_0}{\Delta T},\quad P = \frac{(p+\rho gy)H^2}{\rho\kappa^2 RaPr},$$
$$\vec{R} = \frac{\vec{r}}{H},\quad d\vec{S} = \frac{d\vec{s}}{H},\quad b_a = \frac{\mu_m i}{H},\quad B = \frac{b}{b_a},$$
$$Ra = \frac{g\alpha\Delta T H^3}{\nu\kappa},\quad Pr = \frac{\nu}{\kappa},\quad \gamma = \frac{\chi b_a^2}{\mu_m g H}.$$

It is noted that time is scaled by using the Brunt–Väisälä frequency, $N \equiv (RaPr)^{1/2}\kappa/H^2$, which represents the degree of overall stratification of the fluid. The ratio of magnetizing force to gravity is denoted by γ. The reference value of magnetic field is b_a, which indicates the strength of magnetic field induced by the current in the coil.

The associated boundary conditions are expressed as

$$\begin{aligned} &U = V = \frac{\partial\theta}{\partial Y} = 0 \quad \text{at } Y = 0,1,\\ &U = V = 0,\quad \theta = -0.5 \quad \text{at } X = 0,\\ &U = V = 0,\quad \theta = 0.5 \quad \text{at } X = 1. \end{aligned} \tag{7}$$

The main point of the present study is the time-dependency of the imposed magnetic field. For this purpose, the magnetic field is modeled as a square-wave form, which can be simulated by an on–off switching of the current in the coil. In particular, consideration is given to the cases when the magnetic field is induced alternatively between the two coils, as illustrated in Fig. 1(c). The square-waves are shown by two functions, $F_1(\tau)$ and $F_2(\tau)$, and the non-dimensional period of the square waves is $2\pi/\omega$, i.e.,

$$F_1(\tau) = \begin{cases} 1 & \text{for } 2\pi n/\omega < \tau \leqslant 2\pi n/\omega + \pi/\omega,\\ 0 & \text{for } 2\pi n/\omega + \pi/\omega < \tau \leqslant 2\pi(n+1)/\omega, \end{cases}$$
$$F_2(\tau) = \begin{cases} 0 & \text{for } 2\pi n/\omega < \tau \leqslant 2\pi n/\omega + \pi/\omega,\\ 1 & \text{for } 2\pi n/\omega + \pi/\omega < \tau \leqslant 2\pi(n+1)/\omega, \end{cases}$$

in which n denotes the number of cycles.

Numerical solutions were obtained to the governing equations (3)–(7). The well-documented finite volume

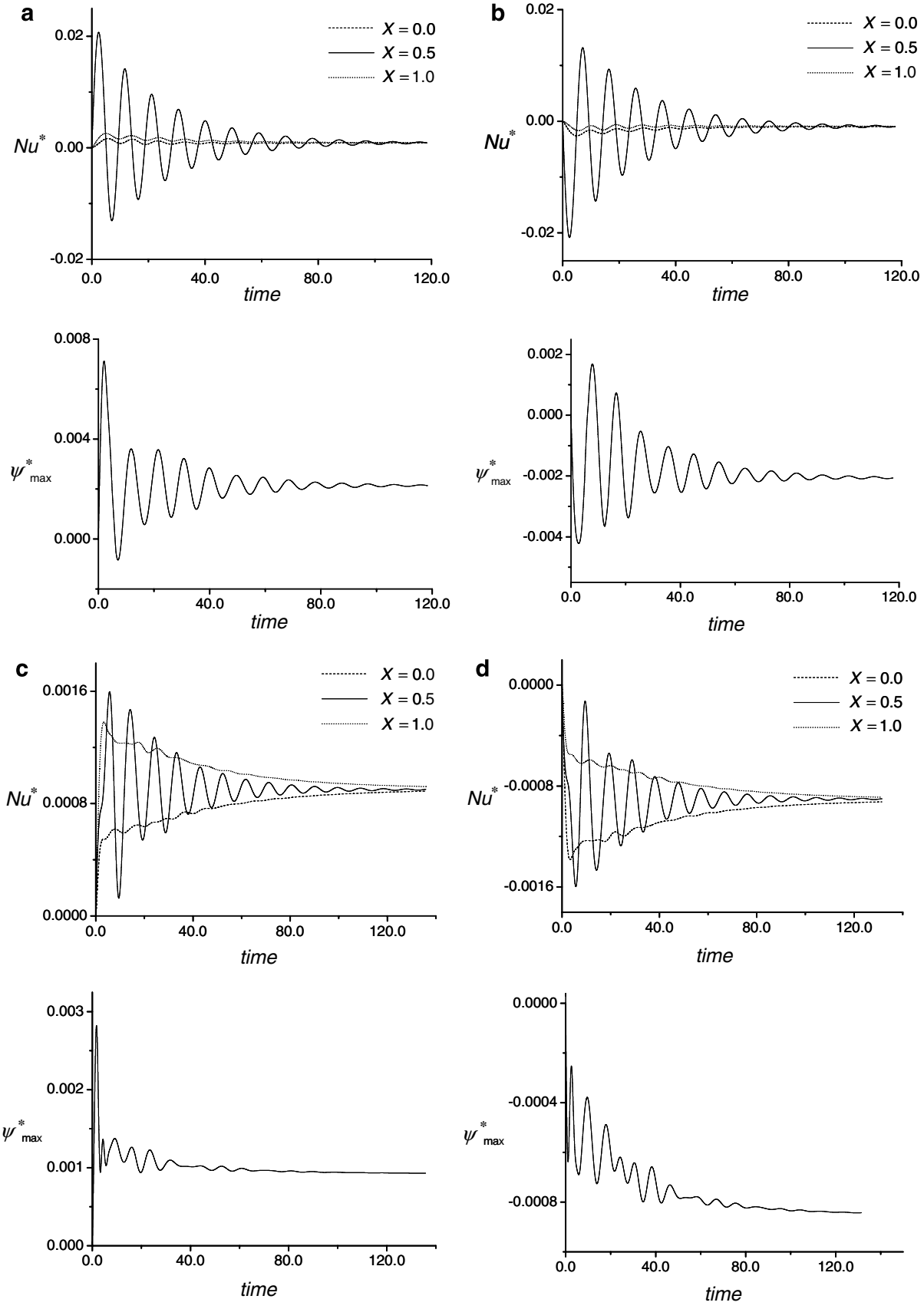

Fig. 2. Time-dependent behavior of normalized Nusselt number and maximum stream function for steady magnetizing force: electric coil is located (a) at the right side of the cavity, (b) at the left side of the cavity, (c) below the cavity and (d) above the cavity.

method based on the SIMPLER algorithm, together with the QUICK scheme, was adopted [16,17]. Each cycle was resolved by 1024 time steps, i.e., $\Delta\tau = 2\pi/(1024\omega)$. The accuracy and robustness of the numerical model was confirmed. The convergence tests for grid, time step and convergence criterion were successful. No claims are made in this study as to the newness and/or innovativeness of the numerical methodologies. The objective is to understand the physical features of flow and heat transfer.

In the present study, it was set that $Ra = 10^7$, $Pr = 0.7$, $A = 1.0$, $0.05 \leqslant \omega \leqslant 4.0$, $e/L = 0.1$, $d/L = 2.0$; and $\gamma = 0.01$ for case 1, and $\gamma = 0.1$ for case 2. These parameter values are in line with the earlier studies of Tagawa et al. [4–6]. For a practical system, it is envisioned that, for air, $T_0 = 293$ K, $H = L = 0.1$ m, $\Delta T = 93.5$ K, $t = 0.182$ s for $\tau = 1$, $b_a = 0.195$ T for $\gamma = 0.01$, and $b_a = 0.616$ T for $\gamma = 0.1$ [4–6]. Extensive computations were also carried out by varying the strength of γ, i.e., in the range of $0.01 \leqslant \gamma \leqslant 0.05$ for case 1, and $0.1 \leqslant \gamma \leqslant 0.5$ for case 2. The results are qualitatively consistent. Therefore, in this paper, the most representative case will be dealt with.

Actual computations were made using more than 30 values of ω. The solutions for the basic steady state of a non-magnetized fluid ($\gamma = 0$) were utilized as the initial conditions.

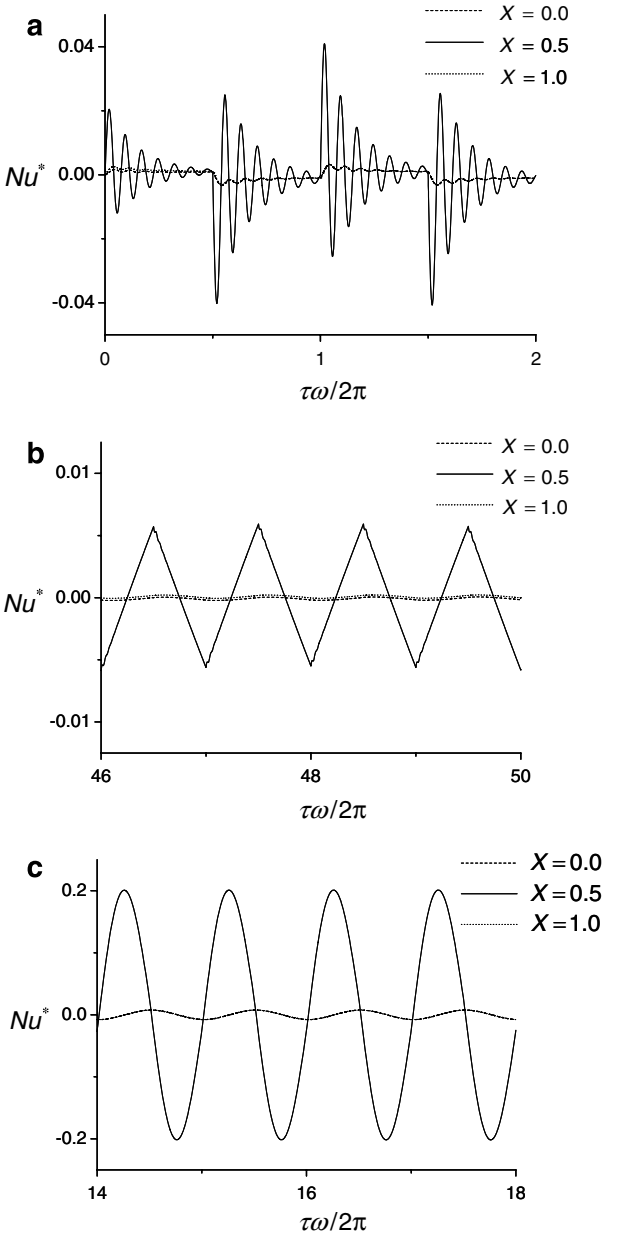

Fig. 3. Time-periodic behavior of the overall Nusselt number (case 1): (a) $\omega = 0.05$, (b) $\omega = 4.0$ and (c) $\omega = 0.67$.

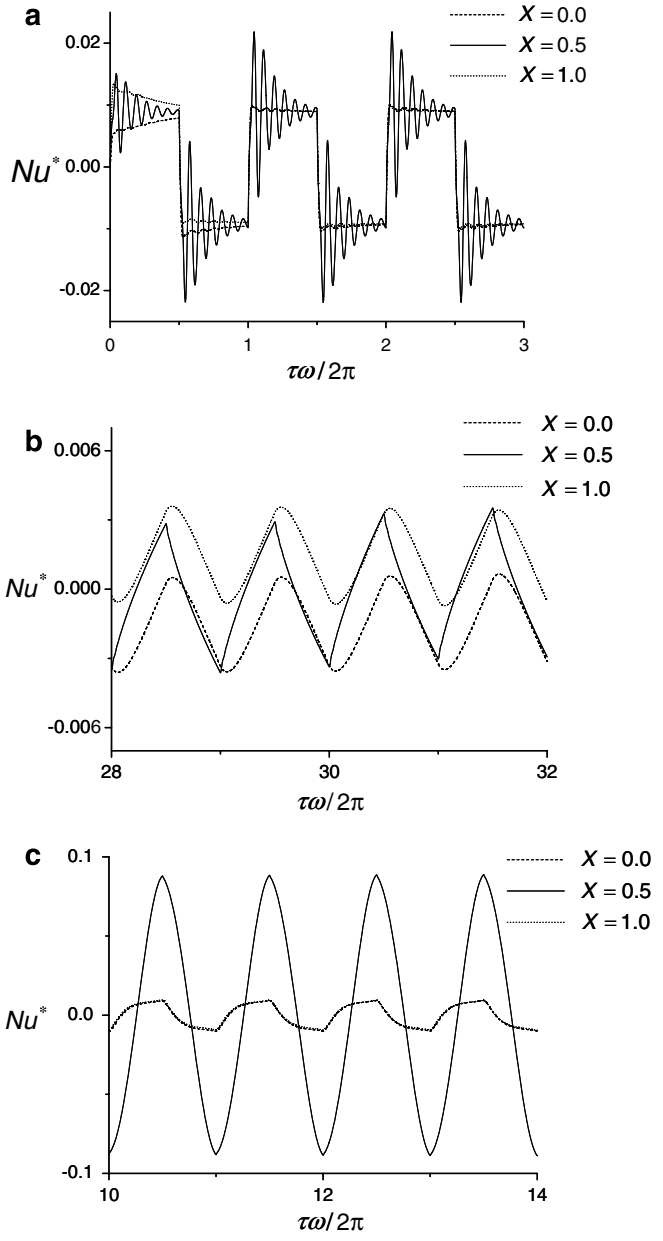

Fig. 4. Time-periodic behavior of the overall Nusselt number (case 2): (a) $\omega = 0.05$, (b) $\omega = 4.0$ and (c) $\omega = 0.66$.

To process the numerical data, it is useful to introduce,

$$\phi^* = \frac{\phi - \phi_{ss}}{\phi_{ss}}, \tag{8}$$

$$A(\phi) = \frac{\mathrm{Max}\{\phi(\tau)\} - \mathrm{Min}\{\phi(\tau)\}}{2} \quad \text{for } \tau_0 \leqslant \tau \leqslant \tau_0 + \frac{2\pi}{\omega}. \tag{9}$$

In the above, ϕ^* indicates the relative departure of the instantaneous value ϕ from the basic-state value ϕ_{ss}. Also, $A(\phi)$ denotes the amplitude of variation of ϕ over a cycle [10]. It follows that the Nusselt number at a vertical plane $X = a$ is given as

$$Nu_{X=a} = \frac{L}{H}\int_0^1 \left[U\theta(RaPr)^{1/2} - \frac{\partial\theta}{\partial X}\right]_{X=a} \mathrm{d}Y. \tag{10}$$

3. Results and discussion

3.1. Effect of geometric arrangement of coil

It is of interest to inquire the effect of coil arrangement. For this purpose, the standard differentially heated steady-state cavity, placed in the gravity field, is adopted. In order to single out the effect of coil geometry, consideration is given to the case when only one coil is placed under steady-state setting. Magnetic field is induced by the steady current in the electric coil.

When the electric coil is located to the right side [Fig. 2(a)] or the lower side [Fig. 2(c)], the values of Nu^* and ψ^*_{max} are greater than the initial-state values, i.e., for $\gamma = 0$. According to Curie's law, the magnetic susceptibility for a paramagnetic substance is inversely proportional to the absolute temperature. Therefore, cold fluid is attracted to the region of high magnetic field, which is close to the electric coil. On the other hand, hot fluid is repelled from the region of high magnetic field. Therefore, when the coil is located to the right side [Fig. 2(a)], the magnetizing force acts like the gravity in the Benard convection. On the other hand, when the coil is located below the cavity [Fig. 2(c)], the role of magnetizing force is to enhance gravity. In these two cases, the overall effect is to intensify convective transports. The suppression of global convective activities is apparent when the coil is placed to the left side of [Fig. 2(b)] or above the cavity [Fig. 2(d)] [note the differences in scales of the ordinates].

3.2. Buoyant convection under time-periodic magnetizing force

For case 1, Fig. 3 shows the time-periodic behavior of the Nusselt numbers at three X-locations, i.e., at the left sidewall (Nu^*_C), at the mid-plane at $X = 0.5$ (Nu^*_M), and at the right sidewall (Nu^*_H).

First, the results for a low-frequency oscillation of magnetizing force, e.g., $\omega = 0.05$, are shown in Fig. 3(a). For this case, the period for the change in magnetizing force is comparable to the global adjustment time of the entire fluid system. After the activation of magnetizing force at one electric coil, the system settles down to a steady state. By this time, the magnetizing force at the other coil is activated, which again leads to another steady state.

Fig. 3(b) illustrates the results for a high-frequency oscillation of magnetizing force, e.g., $\omega = 4.0$. In this case, the changes in the magnetizing force are very rapid; therefore, the overall fluid system does not fully respond to the changes in magnetizing force. The magnitudes of Nu^* are very small throughout the cavity [note the difference in scales for Nu^* in Fig. 3].

Fig. 3(c) demonstrates the amplification of Nu^* in the interior region when the forcing frequency ω is close to the resonance frequency of the system, i.e., $\omega \cong 0.67$.

The computed results for case 2 are illustrated in Fig. 4. The main flow characteristics are qualitatively similar to those of case 1. In passing, it is seen that, under resonance ($\omega \cong 0.66$), there exists a phase difference of 1/4-period from the results of case 1. This is due to the difference in initial time settings of these two cases.

The results of comprehensive numerical computations, using more than 30 different values of ω, are compiled in Fig. 5(a) for case 1 in the plots of $A(Nu^*_M)$ vs. ω. Clearly, $A(Nu^*_M)$, the magnitude of fluctuation of Nu^*_M reaches a

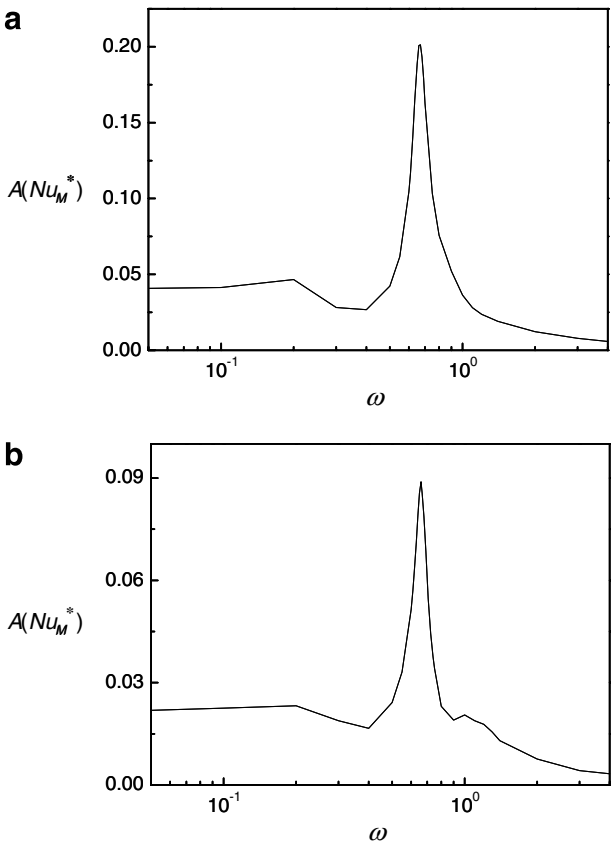

Fig. 5. $A(Nu^*_M)$ variation with ω: (a) case 1 and (b) case 2.

peak value when the forcing frequency is close to the resonance frequency, $\omega \cong \omega_r$ ($\simeq$0.67). When the forcing frequency is far away from ω_r, $A(Nu_M^*)$ is reduced sharply. These are in line with the general pattern of a resonant system [10].

Qualitatively similar results are acquired for case 2, as displayed in Fig. 5(b). The amplitude of fluctuating Nu_M^* takes a peak value at the resonance frequency $\omega \cong \omega_r$ ($\cong$0.66).

The results point to the fact that, in a differentially heated cavity, resonance takes place by tuning in a proper value of frequency of time-varying magnetizing force.

3.3. Identification of the resonance frequency

For a natural convective system, it was shown that the characteristic frequency is characterized by the internal gravity oscillations [10,15]. These oscillation frequencies, in non-dimensionalized form, can be expressed as

$$\omega^I = \frac{C_i}{\sqrt{2}}. \tag{11}$$

In the above, C_i $\left(\approx \sqrt{\partial\theta/\partial y}\right)$ represents the degree of temperature stratification in the interior. In order to estimate C_i, a linear fitting to the vertical temperature profile

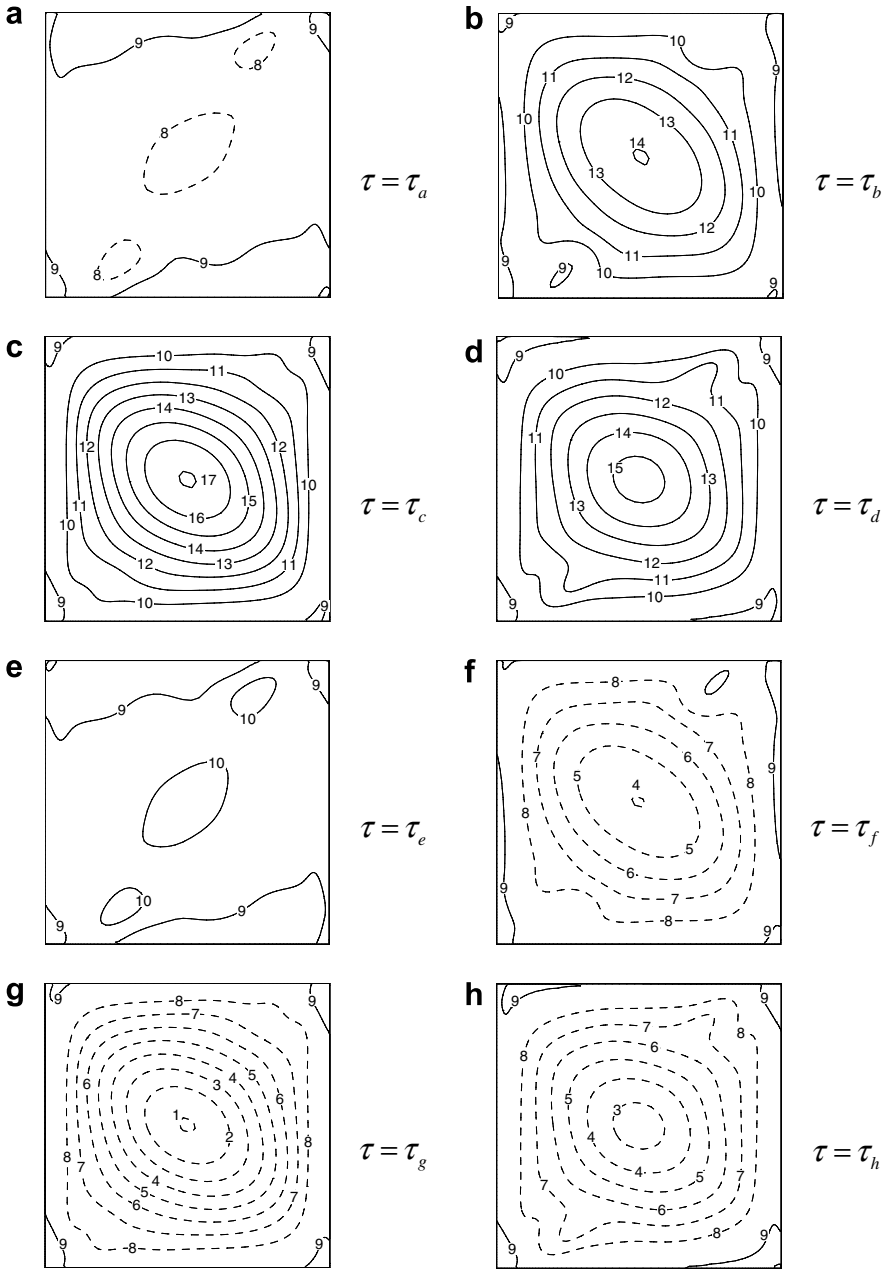

Fig. 6. Sequential plots showing the oscillating part of stream functions under resonance. The contour increments are $\Delta\psi' = 3.25 \times 10^{-4}$. The number, n, in the figures indicates the contour value $(n-9)\Delta\psi'$.

at the mid-plane ($X = 0.5$) is made. For the present cavity layout, $Ra = 10^7$, $Pr = 0.7$, and $C_i \cong 0.96$, which produce $\omega^1 \cong 0.68$. This is in close agreement with the computed value for resonance frequency $\omega_r \cong 0.67$ for case 1, $\omega_r \cong 0.66$ for case 2. In summary, the above-stated numerical and analytical undertakings are consistent with the earlier findings that the resonance frequency is based on the internal gravity oscillations in the cavity.

3.4. Flow characteristics under resonance

It is advantageous to display the departures from the basic state by plotting ψ' ($\equiv \psi - \psi_{ss}$) and θ' ($\equiv \theta - \theta_{ss}$), as suggested by [10]. Here, subscript ss denotes the basic state, i.e., for $F_1(\tau) = F_2(\tau) = 0$.

For convenience, the one period of oscillation is divided into eight intervals. Therefore, at time instants τ_a, τ_b, τ_c, τ_d, $F_1(\tau) = 1.0$ and $F_2(\tau) = 0.0$. On the other hand, at time instants τ_e, τ_f, τ_g, τ_h, $F_1(\tau) = 0.0$ and $F_2(\tau) = 1.0$.

The detailed pictures, depicting the sequential frames of θ' and ψ' under resonance, are shown in Figs. 6 and 7. The qualitative patterns are similar for both case 1 and case 2, and the discussion is focused to case 1. In Fig. 6 at $\tau = \tau_a$, the convective activities begin to be intensified by the magnetizing force. In the bulk of cavity, weak clockwise (CW) flows are seen. At $\tau = \tau_b$, convection strengthens, and

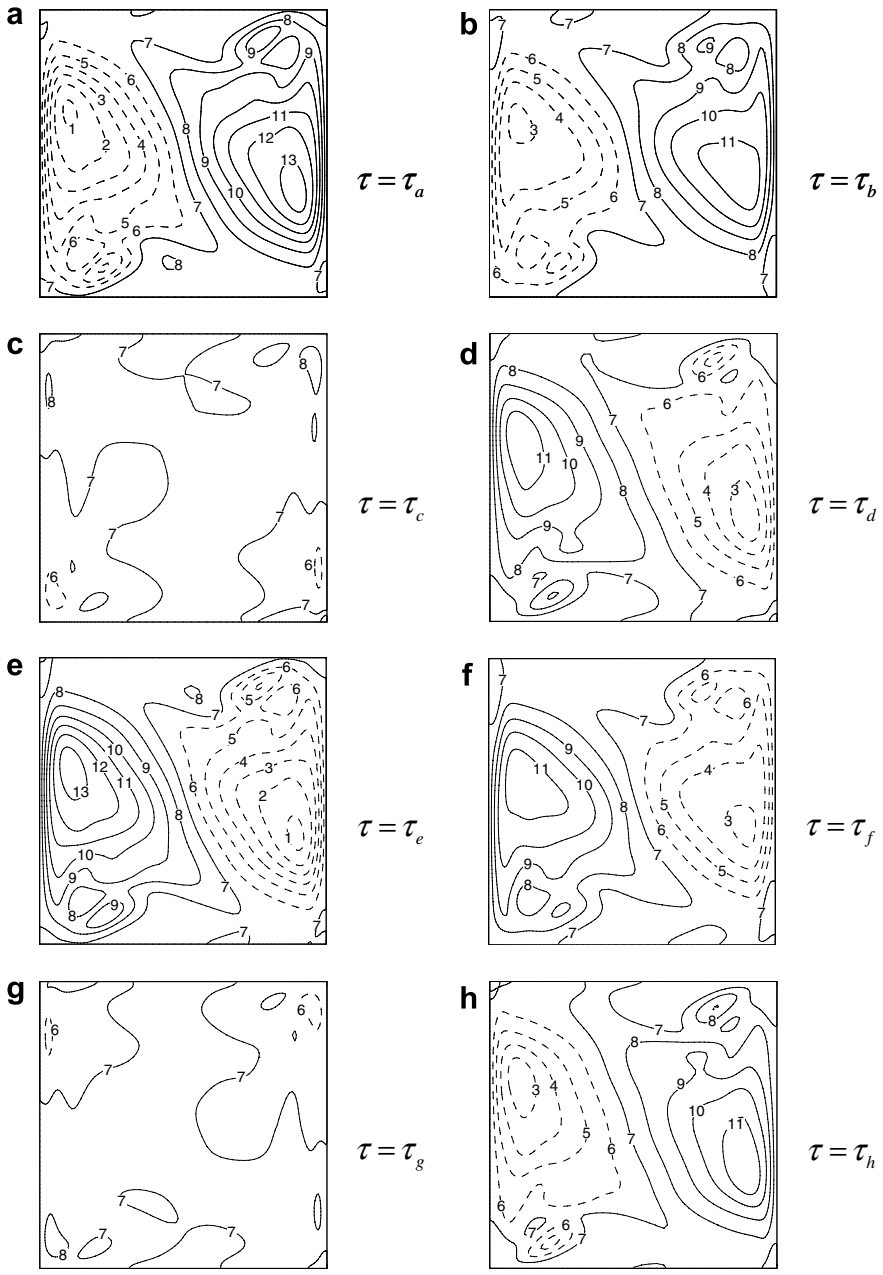

Fig. 7. Sequential plots showing the oscillating part of isotherms under resonance. The contour increments are $\Delta\theta' = 0.02$. The number, n, in the figures indicates the contour value $(n - 7)\Delta\theta'$.

counter-clockwise (CCW) flows are visible. At $\tau = \tau_c$, these CCW flows are most vigorous. After this instant, flows weaken due to the gravity effect while the magnetizing force is still operating. At $\tau = \tau_d$, the CCW flows decrease in strength because of gravity effect. At $\tau = \tau_e$, the magnetizing force acting in the opposite direction suppresses convection. At the same time, CW flows are generated by the gravity effect. At $\tau = \tau_f$, suppression of convection by magnetizing force is apparent, which intensifies CW flows, and these flow features are notable around $\tau = \tau_g$. Afterward, at $\tau = \tau_h$, CW flows weaken due to the gravity effect, which completes a full cycle. In summary, over a period, generation and disappearance of CW and CCW flows in an alternating fashion are captured.

The plots of θ' are given in Fig. 7. At $\tau = \tau_a$, the remaining effects of the previous cycle are visible. At $\tau = \tau_b$, CCW flows are generated by the magnetizing force. This augments convective activities, which brings in hot fluids to the top horizontal boundary layer and interior region. These reduce the difference in temperature in comparison to the basic state. At $\tau = \tau_c$, the above-stated reduction in temperature difference is prominent, and the transport of

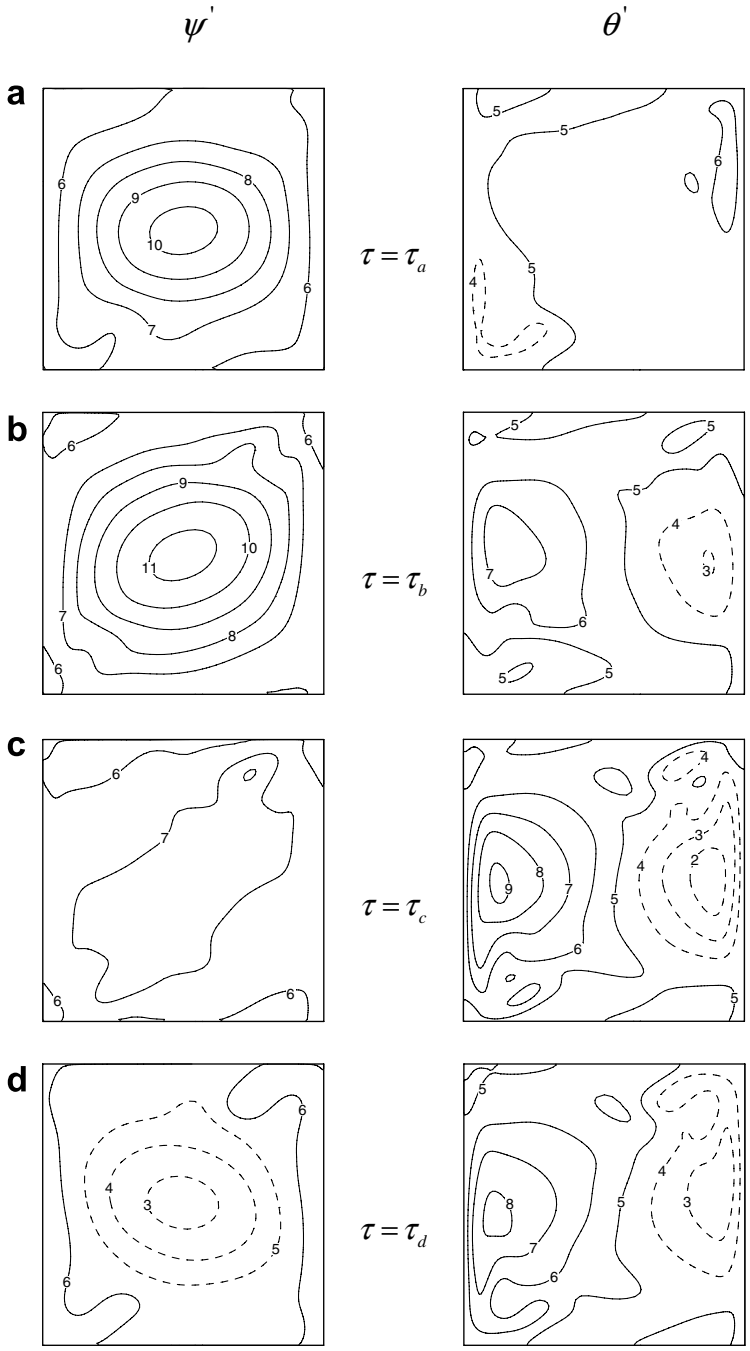

Fig. 8. Same as Figs. 6 and 7, but for $\omega = 0.5$. $\Delta\psi' = 1 \times 10^{-4}$, $(n-6)\Delta\psi'$ and $\Delta\theta' = 0.001$, $(n-5)\Delta\theta'$.

Table 1
Comparison of the results for case 1 and case 2

	Case 1 ($\gamma = 0.01$)	Case 2 ($\gamma = 0.1$)
Resonance frequency (ω_r)	0.67	0.66
$A(Nu^*_M)$	0.2013	0.08891
$A(Nu_M)$	3.34145	1.47581

fluid in the boundary layer is vigorous. At $\tau = \tau_d$, due to intensified convective activities, more hot (cold) fluids are carried in closer to the cold (hot) sidewall. This trend is eminent at $\tau = \tau_e$. Afterward, suppression of convection is in place, and the opposite features are noticed.

Representative sequential plots for θ' and ψ' are given in Fig. 8 under an off-resonance condition, e.g., $\omega \cong 0.5$. In this case, the periods of internal gravity oscillation and of time-periodic magnetizing force do not match. Therefore, enhancement and suppression of convective activities are ineffective. As is obvious, at $\tau = \tau_a$, the magnetizing force acts to augment convection. However, at this time, substantial CCW flows are already in existence due to the gravity effect. At $\tau = \tau_b$, CCW flows are maximized, and, afterward, CCW flows weaken by the action of internal gravity oscillation. At $\tau = \tau_c$, for this particular off-resonance condition, ($\omega = 0.5$), CCW-flows have diminished sharply. At $\tau = \tau_d$, the magnetizing force enhances convection. However, CW flows are generated by internal gravity oscillation. In summary, at times after $\tau = \tau_b$, the actions of magnetic effect and internal gravity oscillations tend to interfere in an opposing fashion.

3.5. Comparisons of case 1 and 2

The numerical data for the foregoing computations are included in Table 1. The strength of magnetic field for case 2 ($\gamma = 0.1$) is 10 times that of case 1 ($\gamma = 0.01$). However, under resonance, the amplitude of fluctuation in Nusselt number for case 1 is more than double that of case 2. This reconfirms that case 1 represents a more robust system which allows more effective control of convective activities. This is expected since case 1 simulates an enclosure of Benard convection configuration.

4. Conclusions

Numerical solutions are acquired to delineate buoyant convection in a sidewall-heated cavity, placed in a uniform gravity field. A time-periodic magnetic field is imposed on the cavity. The electric coils are located to the left and right sides of the cavity for case 1. For case 2, the electric coils are located below and above the cavity. The currents in the coils are activated in an alternating fashion.

The results point to the existence of resonance in the fluid system at a particular value of the frequency of fluctuation in externally applied magnetic field. Under resonance, the amplitude of heat transfer fluctuation shows a peak, and this resonance frequency is characterized by the basic mode of internal gravity oscillation.

Under resonance, the generation and disappearance of counter-clockwise and clockwise flows are apparent. This brings to the augmentation and suppression of convective activities by the action of magnetizing force. Due to these flow patterns, the temperature differences in the system undergo periodic variations. The geometric configuration of case 1 is qualitatively similar to the Benard convection. The heat transfer enhancement is more effective in case 1 than in case 2.

Acknowledgement

This work was supported by the Korea–Poland International cooperative project of KOSEF (Korea Science & Engineering Foundation).

References

[1] D. Braithwaite, E. Beaugnon, R. Tournier, Magnetically controlled convection in paramagnetic fluid, Nature 354 (1991) 134–136.
[2] B. Bai, A. Yabe, J. Qi, N.I. Wakayama, Quantitative analysis of air convection caused by magnetic-fluid coupling, AIAA J. 37 (1999) 1538–1543.
[3] J. Qi, N.I. Wakayama, A. Yabe, Magnetic control of thermal convection in electrically non-conducting or low-conducting paramagnetic fluids, Int. J. Heat Mass Transfer 44 (2001) 3043–3052.
[4] T. Tagawa, R. Shigemitsu, H. Ozoe, Magnetizing force modeled and numerically solved for natural convection of air in a cubic enclosure: effect of the direction of the magnetic field, Int. J. Heat Mass Transfer 45 (2002) 267–277.
[5] R. Shigemitsu, T. Tagawa, H. Ozoe, Numerical computation for natural convection of air in a cubic enclosure under combination of magnetizing and gravitational forces, Numer. Heat Transfer, Part A 43 (2003) 449–463.
[6] T. Tagawa, A. Ujihara, H. Ozoe, Numerical computation for Rayleigh–Benard convection of water in a magnetic field, Int. J. Heat Mass Transfer 46 (2003) 4097–4104.
[7] J.L. Lage, A. Bejan, The resonance of natural convection in an enclosure heated periodically from the side, Int. J. Heat Mass Transfer 36 (1993) 2027–2038.
[8] B.V. Antohe, J.L. Lage, A dynamic thermal insulator: including resonance within a fluid saturated porous medium enclosure heated periodically from the side, Int. J. Heat Mass Transfer 37 (1994) 771–782.
[9] B.V. Antohe, J.L. Lage, Amplitude effect on convection induced by time-periodic horizontal heating, Int. J. Heat Mass Transfer 39 (1996) 1121–1133.
[10] H.S. Kwak, J.M. Hyun, Natural convection in an enclosure having a vertical sidewall with time-varying temperature, J. Fluid Mech. 329 (1996) 65–88.
[11] H.S. Kwak, K. Kuwahara, J.M. Hyun, Prediction of the resonance frequency of natural convection in an enclosure with time-periodic heating imposed on one sidewall, Int. J. Heat Mass Transfer 41 (1998) 3157–3160.
[12] H.S. Kwak, K. Kuwahara, J.M. Hyun, Resonant enhancement of natural convection heat transfer in a square enclosure, Int. J. Heat Mass Transfer 41 (1998) 2837–2846.
[13] K.H. Kim, J.M. Hyun, H.S. Kwak, Buoyant convection in a side-heated cavity under gravity and oscillations, Int. J. Heat Mass Transfer 44 (2001) 857–861.
[14] G. de vahl Davis, I.P. Jones, Natural convection in a square cavity – a comparison exercise, Int. J. Numer. Methods Fluids 3 (1983) 227–248.

[15] S. Paolucci, D.R. Chenoweth, Transition to chaos in a differentially heated vertical cavity, J. Fluid Mech. 201 (1989) 379–410.
[16] S.V. Patankar, Numerical Heat Transfer and Fluid Flow, Hemisphere/McGraw-Hill, New York, 1980.
[17] T. Hayase, J.A.C. Humphrey, R. Greif, A consistently formulated QUICK scheme for fast and stable convergence using finite-volume iterative calculation procedures, J. Comput. Phys. 98 (1992) 108–118.

Further reading

[1] J. Patterson, J. Imberger, Unsteady natural convection in a rectangular cavity, J. Fluid Mech. 100 (1980) 65–86.
[2] J.M. Hyun, Unsteady buoyant convection in an enclosure, Adv. Heat Transfer 34 (1994) 277–320.